Journal Name

RSCPublishing

COMMUNICATION

An Efficient Room Temperature Core-Shell AgPd@MOF Catalyst for Hydrogen Production from Formic Acid

Cite this: DOI: 10.1039/x0xx00000x

Fei Ke,[a,b] Luhuan Wang[a] and Junfa Zhu*[a]

Received 00th January 2012,
Accepted 00th January 2012

DOI: 10.1039/x0xx00000x

www.rsc.org/

A novel core-shell AgPd@MIL-100(Fe) NPs has been fabricated by a facile one-pot method. Significantly, the as-prepared core-shell NPs exhibit much higher catalytic activity than the pure AgPd NPs toward hydrogen production from formic acid without using any additive at room temperature.

One of the most difficult challenges of this century is the sufficient and sustainable supply of clean energy. In this respect, hydrogen has attracted an increasing level of attention as an important clean energy vector and may play a very significant role in power generation in the future.[1] Formic acid (FA) has been studied as a safe and convenient hydrogen storage and generation material due to its high energy density, nontoxicity, and excellent stability at room temperature.[2] FA can be catalytically decomposed to hydrogen and carbon dioxide (CO_2) through a dehydrogenation pathway ($HCOOH \rightarrow H_2 + CO_2$, ΔG_{298K} = -35.0 kJ mol^{-1}).[3] However, carbon monoxide (CO), which is fatally poisonous to catalysts, can also be generated by a dehydration pathway ($HCOOH \rightarrow H_2O + CO$, ΔG_{298K} = -14.9 kJ mol^{-1}).[4] Traditionally, selective dehydrogenation of FA is catalyzed by various homogeneous catalysts of organometallic complexes and the catalysis is enhanced by adding an additive, such as sodium formate or amine adducts.[5] However, the difficulty in the separation of catalysts from the reaction mixture limits the catalysts from scaling-up practical applications. Moreover, the need of additional organic solvents/additives in the FA dedydrogenation is costly, complicated and always involves in toxic substances. To make catalysts more practical for the application in dehydrogenation reaction of FA, heterogeneous catalysts based on noble metal nanoparticles (NPs) have been developed.[6] Unfortunately, these monometallic heterogeneous catalysts are generally more stable but much less active than the homogeneous ones.[2] Recently, bimetallic NP catalysts were reported to show more enhanced activity and stability than their single component counterparts for the dehydrogenation of FA.[7] For example, AgPd NPs supported on cerium oxide[8] or AuPd NPs deposited on activated carbon[9] showed an enhanced FA dehydrogenation activity and selectivity. Despite these tremendous efforts, most of these reported heterogeneous catalysts for the hydrogen generation need the help of extra additives or/and the high temperatures.[10] In this regard, the development of high performance heterogeneous catalysts for hydrogen generation from FA without using any extra additive and at relative low temperatures is of great importance.

Metal-organic frameworks (MOFs) are permanently microporous materials synthesized by assembling metal ions or clusters with polytopic bridging ligands in appropriate solvents.[11] Owing to their high surface area and thermal stability, uniform but tunable pore size and tailorable chemistry,[12] MOFs have been extensively investigated in the past decades and have shown highly promising applications in sensors,[13] drug delivery,[14] gas storage and separation,[15] and catalysis.[16] Recently, by serving as unique host matrices, the potential applications of MOFs can be extended further by encapsulating noble metal NPs within the frameworks.[17] Compared with both pure parent components, this type of composite materials display enhanced catalytic properties due to their synergism effect.[18] Generally, MOFs have been used as functional materials to fabricate composites with noble metal NPs either by using MOFs as templates to generate NPs within their cavities or by encapsulating presynthesized NPs within the MOF layers.[19] Nevertheless, effective control over the dispersibility of MOF-based core-shell structures as well as the morphology and size of the core-shell products still presents significant challenges. So far, there have been a limited number of works about the construction of well-defined noble metal@MOF core-shell structures,[20] and no any prior report on the core-shell noble metal@MOF structures with a bimetallic alloy NPs core coated with a uniform MOF shell.

Herein, we present a facile one-pot method for synthesis of a novel type of porous AgPd@MIL-100(Fe) core-shell NPs with uniform shape and tunable size, in which the bimetallic AgPd alloy NPs core is coated with a uniform MIL-100(Fe) shell (Scheme 1). Impressively, the prepared core-shell AgPd@MIL-100(Fe) NPs with a specific shell thickness exhibit excellent catalytic performance and stability toward hydrogen production from FA without any additives at room temperature.

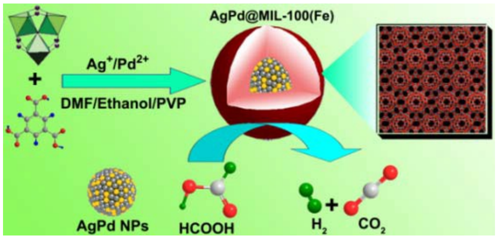

Scheme 1 Schematic representation of synthesis and application of AgPd@MIL-100(Fe) core-shell NPs for FA decomposition at 298 K.

In contrast to previous reports on the presynthesized NPs used as seeds to induce the nucleation of MOF crystals,[19b,21] our strategy relies on a facile one-pot method. Typically, AgPd@MIL-100(Fe) core-shell NPs were prepared by directly mixing the $AgNO_3$, $Pd(NO_3)_2$ and MOF precursors ($FeCl_3$ and H_3BTC) in the reaction solution containing polyvinylpyrrolidone (PVP), N,N-dimethylformamide (DMF), and ethanol. The $AgNO_3$ and $Pd(NO_3)_2$ were first reduced to AgPd alloy NPs by DMF within 20 min at 140 °C.[20,22] Subsequently, MIL-100(Fe) formed and spontaneously grew on the surface of the PVP-modified AgPd NPs, and then uniform core-shell AgPd@MIL-100(Fe) NPs were produced. After 12 h, the reaction mixture was cooled down to room temperature and the product was collected by centrifugation and washed several times with DMF and ethanol. In the above reaction, DMF is the solvent for the H_3BTC solution and determines whether MIL-100(Fe) crystals can be produced. Moreover, it also serves as the reducing agent for the synthesis of AgPd NPs within the core-shell structures.[20]

Fig. S1 (ESI†) shows the typical scanning electron microscope (SEM) images of the as-synthesized AgPd and AgPd@MIL-100(Fe) NPs. These SEM images reveal that both AgPd and AgPd@MIL-100(Fe) NPs are spherical except that the latter has a much larger particle size and a more rugged surface. The morphology and structure of these NPs were further identified by transmission electron microscopy (TEM) and high-angle annular dark-field scanning TEM (HAADF-STEM), as shown in Fig. 1 and Fig. S2 (ESI†). One can see that the AgPd@MIL-100(Fe) NPs have well-defined core-shell nanospherical structures with uniform size and shape, which are in good agreement with the SEM observation. Preliminary statistics based on the products shown in Fig. S1 (ESI†) and Fig. 1 indicates that the size of the core-shell AgPd@MIL-100(Fe) NPs can be tuned from 100 nm (AgPd@MIL-100(Fe)_**A**) to 200 nm (AgPd@MIL-100(Fe)_**B**) and to 250 nm (AgPd@MIL-100(Fe)_**C**), while the diameter of the AgPd NP cores varies from 86 nm to 34 nm and to 14 nm, and correspondingly the shell thickness can be controlled from 7 nm to 83 nm and to 118 nm, respectively, when the added amount of the AgPd precursors in the reaction solution is simply changed. Thanks to the rapid growth rate of the AgPd NP cores compared with the MIL-100(Fe) shells, the less AgPd precursors are added, the smaller AgPd NP cores are produced. Correspondingly, the grown MIL-100(Fe) shells are thicker in the resulting core-shell NPs. The representative high-resolution TEM (HRTEM) image of a single AgPd NP reveals that the distance between two adjacent lattice planes for AgPd NPs is about 0.23 nm (Fig. 1b), which is between the (111) lattice spacing of

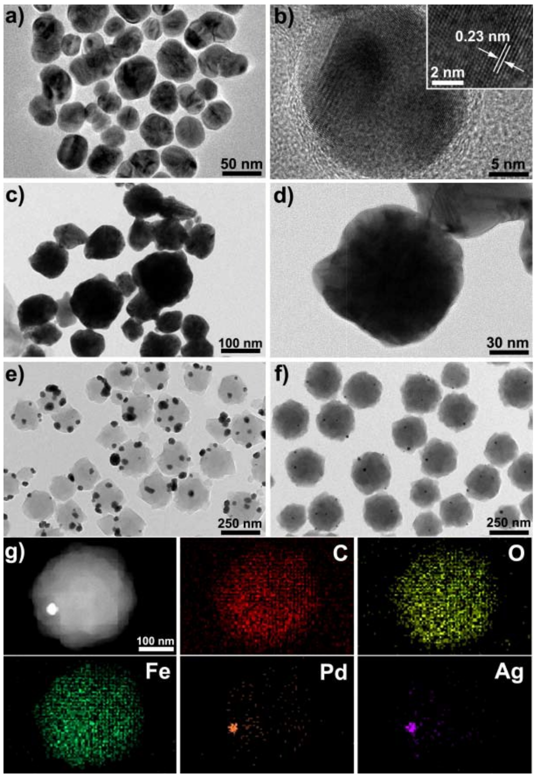

Fig. 1 TEM images of (a) AgPd NPs, (c,d) AgPd@MIL-100(Fe)_**A**, (e) AgPd@MIL-100(Fe)_**B**, (f) AgPd@MIL-100(Fe)_**C**. (b) HRTEM image of AgPd NPs. (g) HAADF-STEM image of an individual core-shell AgPd@MIL-100(Fe)_**C** NP and the corresponding elemental mappings for C, O, Fe, Pd and Ag elements.

face-centered cubic (*fcc*) Ag (0.24 nm) and (*fcc*) Pd (0.22 nm) NPs. Fig. 2 shows the powder X-ray diffraction (PXRD) patterns of the as-prepared AgPd and core-shell AgPd@MIL-100(Fe) NPs. For the AgPd NPs (Fig. 2b), the pattern exhibits well-defined diffraction peaks in the position between the corresponding Ag and Pd peaks, indicating the formation of the AgPd alloy structure.[10] For the products of core-shell AgPd@MIL-100(Fe) NPs (Fig. 2c-e), apart from those diffraction peaks assigned to AgPd NPs, the diffraction peaks belong to MIL-100(Fe) can be detected.[23] For AgPd@MIL-100(Fe) NPs with less AgPd precursors, the diffraction peaks belonging to MIL-100(Fe) become stronger, in agreement with above TEM results. Furthermore, AgPd and core-shell AgPd@MIL-100(Fe) NPs show almost no surface plasmon resonance (SPR) absorption in the UV-vis spectra (Fig. S3, ESI†), which can be attributed to changes in the band structure of the Ag NPs due to alloying with Pd.[10,24] This SPR quenching caused by the alloying effect was also observed in other Ag- and Au-based bimetallic alloy NPs. Finally, the composition of the core-shell structure is particularly obvious in the HAADF-STEM images (Fig. 1g and Fig. S2c, ESI†), in which AgPd alloy NPs as the core appears as brighter contrast due to larger atomic mass. The corresponding elemental mapping further indicates that the Ag and Pd elements are homogeneously located only in the core, while the elements C, O, and Fe of MIL-100(Fe) are homogenously distributed throughout the whole NPs, suggesting that an AgPd core is surrounded with a uniform MIL-100(Fe) shell (Fig. 1g). The corresponding EDX results of point analysis further demonstrate the AgPd-rich core and the MIL-100(Fe)-rich shell (Fig. S2d,e, ESI†). Based on the above experimental analysis, a novel type of AgPd@MIL-

100(Fe) core-shell structures with a AgPd alloy NPs core have been successfully synthesized through the present facile one-pot method.

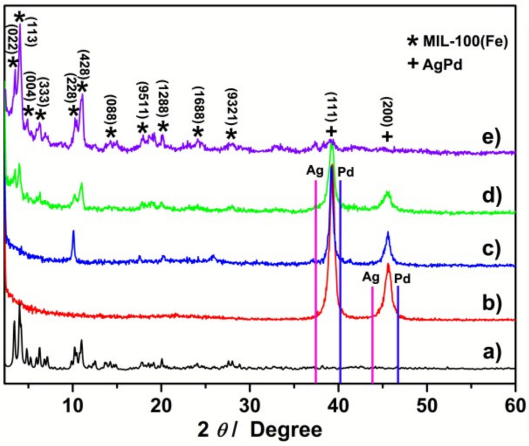

Fig. 2 PXRD patterns of (a) simulated from the crystallographic data of MIL-100(Fe), as-synthesized (b) AgPd NPs, (c) AgPd@MIL-100(Fe)_**A**, (d) AgPd@MIL-100(Fe)_**B**, and (e) AgPd@MIL-100(Fe)_**C**.

The features of the MOF shells, especially the porosity, determine the properties of the core-shell NPs.[20] N_2 adsorption-desorption isotherms measurements were undertaken to verify the porous nature of all the obtained core-shell AgPd@MIL-100(Fe) NPs and to calculate their surface areas. The results are shown in Fig. S4 (ESI†). It can be found that the Brunauer-Emmett-Teller (BET) surface areas and pore volumes of the samples increased significantly with decreasing the amount of AgPd precursors in the reaction solution. The BET surface areas of the core-shell AgPd@MIL-100(Fe) NPs increases from 6.1 $m^2\ g^{-1}$ to 1036.9 $m^2\ g^{-1}$, and pore volume increases from 0.01 $cm^3\ g^{-1}$ to 0.72 $cm^3\ g^{-1}$, respectively (Table S1, ESI†), due to the decreasing contribution of nonporous AgPd NP cores to the mass of core-shell NPs. Furthermore, estimation of the pore size distribution by density functional theory (DFT) shows two pore systems at 1.59 and 2.16 nm for AgPd@MIL-100(Fe) core-shell NPs (Fig. S4b, ESI†), attributed to micropore and mesopore cages, respectively, which is consistent with the previously reported results for MIL-100(Fe) crystals.[26] Moreover, as the shell thickness increases, the corresponding pore size intensity of the core-shell NPs increases gradually, consistent with the results of BET analysis. The chemical composition of the core-shell NPs is also directly evidenced by energy dispersive X-ray (EDX) spectra. As can be seen from Fig. S5 (ESI†), AgPd@MIL-100(Fe) NPs are composed of Ag, Pd, C, O, and Fe elements. With increasing the shell thickness of MIL-100(Fe), the signals of Ag and Pd elements in the AgPd@MIL-100(Fe) NPs decrease gradually, while the signals of C, O, and Fe elements of MIL-100(Fe) increase, which is in good agreement with the compositional changes occurring during the reactions.

Next, FA decomposition is employed for evaluating the catalytic activities of the AgPd@MIL-100(Fe) catalysts. Reaction was initiated by introducing FA aqueous solution into the quartz reaction cell containing the as-synthesized AgPd@MIL-100(Fe) catalysts with vigorous stirring at room temperature. Hydrogen generated from the FA decomposition was analyzed by an on-line gas chromatograph. Fig. 3 shows the catalytic activities of the core-shell AgPd@MIL-100(Fe) NPs together with the bare AgPd NPs for hydrogen production from FA decomposition at 298 K. Obviously, the AgPd@MIL-100(Fe) NPs exhibit high catalytic activity in hydrogen generation from FA. As can be seen, under the same evaluation conditions, the AgPd@MIL-100(Fe)_**A** with a shell thickness of 7 nm shows the highest activity among all the prepared catalysts (Fig. 3), suggesting that the MIL-100(Fe) shell and its thickness exhibit a significant influence on the catalytic activity of the AgPd@MIL-100(Fe) NPs. For the AgPd@MIL-100(Fe)_**A**, the 7 nm shell is thin enough, allowing not only the adsorption of FA molecules but also the fast mass transfer of FA to the embedded AgPd core. If the shell is too thick, such as the cases of AgPd@MIL-100(Fe)_**B** and AgPd@MIL-100(Fe)_**C**, where the shell thicknesses are 83 nm and 118 nm, respectively, the diffusion of FA into the interface of the AgPd core becomes difficult, which is believed to be responsible for the decreased catalytic efficiency. However, for bare AgPd NPs, although the diffusion of FA into the interface is easy, the enrichment of FA molecules nearby the AgPd NPs is absent.[20] While in the blank experiment with pure MIL-100(Fe), no gas evolution is detected, indicating no activity of pure MIL-100(Fe) in the FA decomposition reaction. This comparison demonstrates that the drastic dehydrogenation activity enhancement of the AgPd@MIL-100(Fe)_**A** NPs is realized only by the combination of AgPd NPs and porous MIL-100(Fe) in the specific core-shell structure. This is consistent with what was observed on the Au@SiO_2_EN(AP) systems.[27] Significantly, the initial turnover frequency [TOF, Equation S2, ESI†] value for the AgPd@MIL-100(Fe)_**A** was calculated to be 5[illegible] h^{-1} (Table S1, ESI†), which is three times higher than that of bare AgPd NPs. This value is superior to many of reported heterogeneous catalysts for this reaction without additives at room temperature,[3,7] and even comparable to some of those with additives and/or at the elevated temperatures (Table S2, ESI†).[8,27-28] Furthermore, the initial rate of hydrogen generation [Equation S3, ESI†] is determined to be 13.25 L $H_2\ h^{-1}\ g_{Ag+Pd}^{-1}$. Such hydrogen output corresponds to a theoretical power density of 17.90 W $h^{-1}\ g_{Ag+Pd}^{-1}$ for energy generation.[3,28a] Therefore, 0.037-0.15 g of the present AgPd@MIL-100(Fe)_**A** catalyst would be sufficient to supply hydrogen for the small proton exchange membrane (PEM) fuel cell devices (0.5-2.0 Wh).[3,28a]

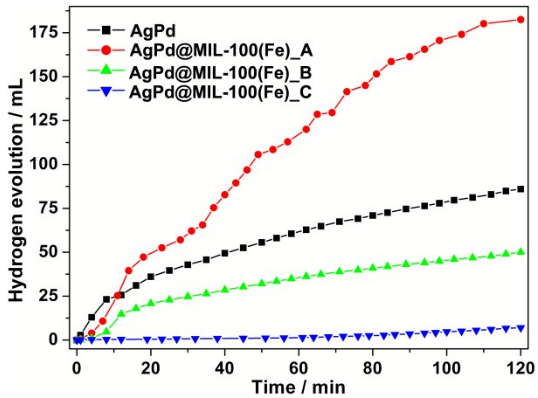

Fig. 3 Hydrogen generation by decomposition of FA (1 M, 10 mL) versus time in the presence of AgPd and core-shell AgPd@MIL-100(Fe) NPs at 298 K.

Considering that the AgPd NPs of the prepared pure AgPd bimetallic catalyst has the similar shape but smaller size compared with the AgPd@MIL-100(Fe)_**A** core-shell catalyst (Fig. 1), the enhanced catalytic performance of AgPd@MIL-100(Fe)_**A** may be attributed to its special core-shell structure. And this has been further supported by the fact that the physical mixture of pure AgPd and MIL-100(Fe) (mass ratio of AgPd:MIL-100(Fe) is 75:25) for the same reaction exhibits much lower activity (Fig. S6, ESI†) than that of AgPd@MIL-100(Fe)_**A.** Because of the synergistic effect between Ag and Pd in the AgPd alloy structure, the adsorption of CO on Pd is inhibited, which consequently prolongs the lifetime of the catalyst.[10] According to previous reports,[6,27,28] the FA decomposition process can be elucidated as the following steps: (1) Dissociation of the O-H bond of FA at the metal surface, affording an metal formate species with an H^+ ion. (2) Metal formate species undergo β-hydride elimination to produce CO_2 and a metal hydride species. (3) The hydride species react with the H^+ ions to form hydrogen molecular. Here, the FA molecules can be adsorbed onto the porous MIL-100(Fe) shell,[18,28d] which provides a high concentration of FA near the AgPd core, leading to highly efficient contact between them and thus enhances the catalytic efficiency of the FA decomposition. Additionally, the O-H bond cleavage is facilitated with the assistance of the Lewis acid activity metal center of the MIL-100(Fe). Therefore, it is reasonable to understand that the core-shell AgPd@MIL-100(Fe)_**A** NPs show relatively higher catalytic activity than AgPd NPs alone.

The stability is important for the practical application of catalysts. We further performed a brief stability test for the core-shell AgPd@MIL-100(Fe)_**A** catalyst in the dehydrogenation reaction of FA at room temperature. In this experiment, the catalyst was recovered from the solution after the reaction completion for the next round of reaction under the same conditions. The results show that the productivity of hydrogen remain almost unchanged after five runs (Fig. S7, ESI†). Moreover, after the reaction, the PXRD diffraction pattern, shown in Fig. S8 (ESI†), remains almost unchanged after the five consecutive reuses, suggesting that the crystal structure of the AgPd@MIL-100(Fe)_**A** is not damaged upon its reuse as a heterogeneous catalyst. Furthermore, the TEM investigations show no obvious change in both size and morphology after multiple use in catalysis (Fig. S9, ESI†). The uniform distribution of AgPd alloy NP core without aggregation after catalytic reaction confirms the advantage of the confinement effect of the MOF shell. These findings indicate that the core-shell AgPd@MIL-100(Fe)_**A** catalyst was stable under the current FA dehydrogenation condition and could be reused for multiple rounds of the dehydrogenation reaction.

In summary, we have for the first time demonstrated a facile one-pot method for the fabrication of a novel core-shell AgPd@MIL-100(Fe) NPs, which were used as highly efficient catalysts in the generation of hydrogen from FA decomposition without using any additive at room temperature. Compared with bare AgPd NPs, the core-shell AgPd@MIL-100(Fe) NPs synergistically improves the catalytic activity for the dehydrogenation of FA in aqueous solution. Furthermore, this high catalytic activity remains almost unchanged after multiple rounds of the dehydrogenation reaction. Therefore, these new types of MOF-based bimetallic core-shell nanocatalysts might lead to a new approach to further develop economic and highly efficient catalysts for the hydrogen production from FA to meet the requirement of practical application of FA as a hydrogen storage/generation material.

This work is supported by the National Basic Research Program of China (2010CB923302, 2013CB834605), the National Natural Science Foundation of China (Grant Nos. U1232102), and the Youth Research Foundation of Anhui Agricultural University (2014zr001).

Notes and references

[a]National Synchrotron Radiation Laboratory and Collaborative Innovation Center of Suzhou Nano Science and Technology, University of Science and Technology of China, Hefei 230029, P. R. China. E-mail: jfzhu@ustc.edu.cn

[b]Department of Applied Chemistry, Anhui Agricultural University, Hefei 230036 (P.R. China).

† Electronic Supplementary Information (ESI) available. See DOI: 10.1039/c000000x/

1 J. F. Hull, Y. Himeda, W.-H. Wang, B. Hashiguchi, R. Periana, D. J. Szalda, J. T. Muckerman and E. Fujita, *Nat. Chem.*, 2012, **4**, 383.
2 M. Grasemann and G. Laurenczy, *Energy Environ. Sci.*, 2012, **5**, 817
3 Z.-L. Wang, J.-M. Yan, Y. Ping, H.-L. Wang, W.-T. Zheng and Q. Jiang, *Angew. Chem. Int. Ed.*, 2013, **52**, 4406.
4 C. Hu, S.-W. Ting, J. Tsui and K.-Y. Chan, *Int. J. Hydrogen Energy*, 2012, **37**, 6372.
5 B. Loges, A. Boddien, H. Junge and M. Beller, *Angew. Chem. Int. Ed.*, 2008, **47**, 3962.
6 M. Ojeda and E. Iglesia, *Angew. Chem. Int. Ed.*, 2009, **48**, 4800.
7 K. Tedsree, T. Li, S. Jones, C. W. A. Chan, K. M. K. Yu, P. A. J. Ba..., E. A. Marquis, G. D. W. Smith and S. C. E. Tsang, *Nat. Nanotechnol.*, 2011, **6**, 302.
8 X. Zhou, Y. Huang, W. Xing, C. Liu, J. Liao and T. Lu, *Chem. Commun.*, 2008, 3540.
9 O. Metin, X. Sun and S. Sun, *Nanoscale*, 2013, **5**, 910.
10 S. Zhang, O. Metin, D. Su and S. Sun, *Angew. Chem. Int. Ed.*, 2013, **52**, 3681.
11 H. C. Zhou, J. R. Long and O. M. Yaghi, *Chem. Rev.*, 2012, **112**, 67
12 W.-w. Zhan, Q. Kuang, J.-z. Zhou, X.-j. Kong, Z.-x. Xie and L.-s. Zheng, *J. Am. Chem. Soc.*, 2013, **135**, 1926.
13 S. S. Nagarkar, B. Joarder, A. K. Chaudhari, S. Mukherjee and S. K. Ghosh, *Angew. Chem. Int. Ed.*, 2013, **52**, 2881.
14 P. Horcajada, R. Gref, T. Baati, P. K. Allan, G. Maurin, P. Couvreur, G. Ferey, R. E. Morris and C. Serre, *Chem. Rev.*, 2012, **112**, 1232.
15 J. R. Li, J. Sculley and H. C. Zhou, *Chem. Rev.*, 2012, **112**, 869.
16 A. Dhakshinamoorthy, M. Alvaro and H. Garcia, *Chem. Commun.*, 2012, **48**, 11275.
17 G. Lu, S. Z. Li, Z. Guo, O. K. Farha, B. G. Hauser, X. Y. Qi, Y. Wang, X. Wang, S. Y. Han, X. G. Liu, J. S. DuChene, H. Zhang, Q. C. Zhang, X. D. Chen, J. Ma, S. C. J. Loo, W. D. Wei, Y. H. Yang, J. T. Hupp and F. W. Huo, *Nat. Chem.*, 2012, **4**, 310.
18 X. Gu, Z.-H. Lu, H.-L. Jiang, T. Akita and Q. Xu, *J. Am. Chem. Soc.*, 2011, **133**, 11822.
19 a) Q.-L. Zhu, J. Li and Q. Xu, *J. Am. Chem. Soc.*, 2013, **135**, 10210; b) C.-H. Kuo, Y. Tang, L.-Y. Chou, B. T. Sneed, C. N. Brodsky, Z. Zhao and C.-K. Tsung, *J. Am. Chem. Soc.*, 2012, **134**, 14345.
20 L. He, Y. Liu, J. Liu, Y. Xiong, J. Zheng, Y. Liu and Z. Tang, *Angew. Chem. Int. Ed.*, 2013, **52**, 3741.
21 K. Sugikawa, Y. Furukawa and K. Sada, *Chem. Mater.*, 2011, **23**, 313
22 I. Pastoriza-Santos and L. M. Liz-Marzan, *Adv. Funct. Mater.*, 2009, **19**, 679.
23 P. Horcajada, S. Surble, C. Serre, D. Y. Hong, Y. K. Seo, J. S. Chang, J. M. Greneche, I. Margiolaki and G. Ferey, *Chem. Commun.*, 200..., 2820.

24 J. Feng, C. Ma, P. J. Miedziak, J. K. Edwards, G. L. Brett, D. Li, Y. Du, D. J. Morgan and G. J. Hutchings, *Dalton Trans.*, 2013, **42**, 14498.
25 H. Rong, S. Cai, Z. Niu and Y. Li, *ACS Catal.*, 2013, **3**, 1560.
26 F. Ke, L.-G. Qiu, Y.-P. Yuan, X. Jiang and J.-F. Zhu, *J. Mater. Chem.*, 2012, **22**, 9497.
27 M. Yadav, T. Akita, N. Tsumori and Q. Xu, *J. Mater. Chem.*, 2012, **22**, 12582.
28 a) Q.-Y. Bi, X.-L. Du, Y.-M. Liu, Y. Cao, H.-Y. He and K.-N. Fan, *J. Am. Chem. Soc.*, 2012, **134**, 8926; b) S.-W. Ting, S. Cheng, K.-Y. Tsang, N. van der Laak and K.-Y. Chan, *Chem. Commun.*, 2009, 7333; c) Y. Huang, X. Zhou, M. Yin, C. Liu and W. Xing, *Chem. Mater.*, 2010, **22**, 5122; d) M. Martis, K. Mori, K. Fujiwara, W.-S. Ahn and H. Yamashita, *J. Phys. Chem. C*, 2013, **117**, 22805.